Int. J. Heat Mass Transfer. Vol. 36, No. 12, pp. 3017–3027, 1993
Printed in Great Britain

0017-9310/93 $6.00+0.00

Investigation of solutal convection during the dissolution of silicon in a sandwich system

S. ERBAY, H. A. ERBAY, N. DJILALI and S. DOST
Centre for Advanced Materials and Related Technology and Department of Mechanical Engineering, University of Victoria, Victoria, B.C., Canada V8W 3P6

(*Received* 21 *October* 1992 *and in final form* 5 *January* 1993)

Abstract—This paper considers natural convection due to solutal gradients during the dissolution of silicon in a substrate–solution–substrate 'sandwich' system under isothermal conditions. This work is motivated by the need to understand the role of convection in liquid-phase epitaxial growth of semiconductor crystals. Unsteady two-dimensional numerical simulations are presented for two dissolution experiments. Solutal convection is found to be predominant during the initial phase of the process and causes a rapid increase in the dissolution depths of both substrates. However, because convection is mostly confined to the lower half of the sandwich system, lower substrate dissolution depths are about twice as large. This result is in good agreement with available experimental data. Another interesting consequence of convection is the development of a wavy irregular surface along the lower substrate.

1. INTRODUCTION

SEMI-CONDUCTING crystals such as silicon (Si) and gallium arsenide (GaAs) form the core of a number of electronic and electro-acoustic devices. The study of growth techniques for these crystals is therefore of considerable technological significance. A commonly-used growth method to produce compound semi-conductor crystals from a solution is Liquid Phase Epitaxy (LPE). The main advantages of this growth technique are controlled growth on seed crystals from high temperature solutions, and the possibility of growing high quality films on a variety of substrates [1]. Furthermore, recent developments [2] indicate that this technique could be use to produce large single crystals which are required in a growing body of applications in high power electronic devices and in laser technology.

LPE consists of depositing thin layers of crystalline material from a dilute solution onto a substrate of similar composition. Gradual reduction of the temperature of the solution results in a reduction of the saturation concentration and causes crystallization of the excess solute (i.e. silicon in the case of an indium-silicon solution) onto the substrate. Because of its importance in the growth of semiconductor crystals used in electronic device fabrication, a number of theoretical models of the LPE process have been developed to predict solute concentration distributions, growth rate and maximum allowed cooling rate for growth with no interface instability. Most of these models (e.g. [2–4]) are based on the assumption that epitaxial growth is controlled by diffusive transport in the solution. This effectively restricts the validity of the models to zero-gravity conditions [4, 5]. Little attention has been paid to the analysis of natural convection during growth and dissolution of crystals despite experimental evidence documenting its importance.

In a recent study [6], the effect of convection on both dissolution and epitaxial growth of silicon in an In–Si system has been investigated experimentally. A horizontal 'sandwich' system consisting of a substrate–solution–substrate arrangement was used. In both the dissolution and growth experiments the substrates and solution were uniformly heated to an initial temperature; the indium solution, saturated with silicon at the initial temperature, was then inserted between upper and lower substrates. Subsequently the temperature of the solution was increased or decreased to the final temperature for the dissolution or growth experiments, respectively. It was observed that dissolution of silicon occurs mainly on the lower substrate, while growth on the upper substrate is larger than that for the lower substrate. This phenomenon was attributed to the solutal convection driven by solute concentration gradients. Based on these results a new growth technique which modulates the solution temperature periodically with an appropriate amplitude was proposed and it was concluded that, using this technique, an epitaxial layer with a desirable thickness can be grown.

In another study by the same group [7], a different dissolution experiment was carried out using the same horizontal sandwich arrangement. In that experiment, the substrates and indium solvent were uniformly heated up to the dissolution temperature. The indium solvent was then inserted between the silicon substrates and the dissolution of silicon was observed at that temperature. Again, the dissolution depth of the

NOMENCLATURE

C	concentration of silicon	Greek symbols	
D	diffusion coefficient	β	solutal expansion coefficient
H	dissolution depth	ΔH	heat of fusion
p	static pressure	ν	kinematic viscosity
R	gas constant	ρ	density
T	temperature	Ψ	stream function.
t	time		
u, v	horizontal and vertical velocity components	Subscripts	
X	mole fraction of silicon in liquid phase	I	interface value
		In	value for indium
		M	melting point value
x, y	horizontal and vertical coordinates.	Si	value for silicon
		0	initial value.

lower substrate was found to be higher than that of the upper. A numerical simulation using a stream function–vorticity formulation was also presented in the same paper. This simulation was limited by the assumption of an infinitely wide cell (i.e. side wall effects were neglected). Nevertheless, the results confirmed the importance of solutal convection.

In the temperature modulation growth technique proposed by Sukegawa *et al.* [6], natural convection is used to sustain growth by combining dissolution and growth cycles. The present research is motivated by the potential of this new technique for growing epitaxial layers of any desirable thickness. The focus of this work is to improve our understanding of mass transfer and natural convection in the dissolution and LPE processes. This paper presents the results of a numerical study of the dissolution process in a horizontal In–Si sandwich system (Fig. 1) consisting of a substrate–solution–substrate arrangement. The numerical simulations were performed by solving the two-dimensional time-dependent Navier–Stokes and mass transport equations using a finite-volume method. Computed flow and concentration fields are presented for two dissolution experiments, and the effects of solutal convection on the dissolution rate and shape of the substrates are discussed. Predictions are also presented for dissolution under microgravity conditions.

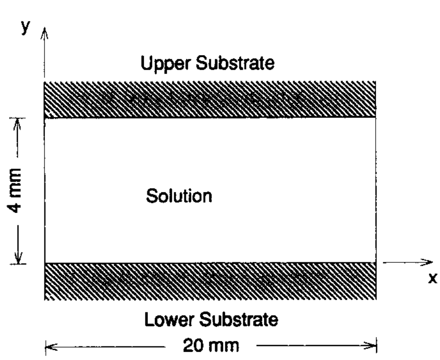

FIG. 1. Schematic view of the sandwich system.

2. PROBLEM FORMULATION

2.1. *Experimental background*

The simulations were performed for two cases corresponding to experiments performed in the 'sandwich' system shown in Fig. 1. This consisted of two horizontal silicon substrates set face to face, 4 mm apart, in a graphite boat. The two experiments considered are: (i) dissolution experiment of Kimura *et al.* [7]; and (ii) dissolution experiment of Sukegawa *et al.* [6].

In the first experiment, the substrates and the indium solvent were uniformly heated to 974°C. The indium solvent was then inserted between upper and lower substrates and was maintained at a uniform temperature for one hour. At the end of this period, the dissolution of the lower substrate was observed to be greater than that of the upper substrate, implying that the melt saturation is achieved through silicon atoms originating mostly from the lower substrate.

In the second dissolution experiment, the silicon saturated indium solution, at an initial temperature of 994°C, was inserted between upper and lower substrates. The temperature of the solution was then brought up to a final temperature of 1020°C, and maintained at a uniform temperature for 150 min. At the end of this period, the dissolution of the lower substrate was again observed to be greater than that of the upper substrate. In both dissolution experiments, it was suggested that the difference in dissolution depths arises from the difference in specific gravity between silicon and indium, with the specific gravity of indium estimated to be 2.5 times that of silicon at the dissolution temperature.

2.2. *Governing equations and boundary conditions*

In general, macroscopic dissolution of an epitaxial layer is affected by mass and heat transfer as well as fluid flow. In the physical problem considered here, the temperature was kept constant within 0.25°C, and the process is therefore assumed to be isothermal. The indium solution is assumed to be an incompressible, Newtonian fluid. We also use the Boussinesq approximation (i.e. the density of the solution is constant in all equations except in the gravitational term of the momentum equation), and we assume that the process is nominally two-dimensional.

Under these conditions, the governing equations expressing conservation of mass, momentum and solute concentration take the following form in Cartesian coordinates:

Incompressibility

$$\frac{\partial u}{\partial x}+\frac{\partial v}{\partial y}=0 \tag{1}$$

Momentum

$$\frac{\partial u}{\partial t}+u\frac{\partial u}{\partial x}+v\frac{\partial u}{\partial y}=-\frac{1}{\rho_0}\frac{\partial p}{\partial x}+\nu\left(\frac{\partial^2 u}{\partial x^2}+\frac{\partial^2 u}{\partial y^2}\right) \tag{2}$$

$$\frac{\partial v}{\partial t}+u\frac{\partial v}{\partial x}+v\frac{\partial v}{\partial y}=-\frac{1}{\rho_0}\frac{\partial p}{\partial y}+\nu\left(\frac{\partial^2 v}{\partial x^2}+\frac{\partial^2 v}{\partial y^2}\right)-\beta(C-C_0)g \tag{3}$$

Mass Transport

$$\frac{\partial C}{\partial t}+u\frac{\partial C}{\partial x}+v\frac{\partial C}{\partial y}=D\left(\frac{\partial^2 C}{\partial x^2}+\frac{\partial^2 C}{\partial y^2}\right) \tag{4}$$

where u and v are the velocity components in the x and y directions, respectively, t is time, p is the pressure, C is the silicon concentration in the solution, ρ_0 is the density of the solution, ν is the kinematic viscosity, β is the solutal expansion coefficient, C_0 is the initial concentration of silicon, D is the diffusion coefficient and g is the gravitational constant.

A dissolving crystal gives rise to a moving boundary problem. However, the changes in the substrate thicknesses during the dissolution process are very small compared to the distance between upper and lower substrates. It is therefore assumed, as a first approximation, that the interfaces are fixed. We also assume that the interface concentration is given by the solubility relation [8].

The initial and boundary conditions corresponding to the dissolution experiments [6, 7] are given by:

Initial conditions

$$u=v=0,\quad p=p_0,\quad C=C_0\quad \text{at } t=0. \tag{5}$$

Boundary conditions on vertical walls

$$u=v=0,\quad \frac{\partial C}{\partial x}=0. \tag{6}$$

Interface conditions on horizontal boundaries

$$u=v=0,\quad C=C_{\mathrm{I}}. \tag{7}$$

The values of the concentrations C_0 and C_{I} depend on the case being simulated:

1. *First dissolution experiment*: $C_0 = 0$ and C_{I} is equal to the solute concentration calculated from the solubility relation at a dissolution temperature of 974°C.
2. *Second dissolution experiment*: C_0 is equal to the initial solute concentration calculated from the solubility relation at an initial temperature of 994°C, and C_{I} is the solute concentration calculated at a dissolution temperature of 1020°C.

The dissolution depth was calculated at the end of each time step using the interface relation given by Wilcox [9]:

$$H(t)=\frac{\rho D}{\rho_{\mathrm{Si}}}\int_0^t\frac{1}{1-C}\frac{\partial C}{\partial y}\,\mathrm{d}t. \tag{8}$$

This relation, which represents conservation of solute at the interface, can be obtained as a jump condition in the derivation of the field equations [9].

The parameters used in the computations are listed in Table 1. These values were obtained using the relations given in the Appendix.

2.3. *Numerical solution procedure*

The conservation equations (1)–(4) are solved numerically using a control volume method. The equations are discretized using a hybrid central/upwind discretization scheme [10] on a staggered grid non-uniform grid system, whereby velocity nodes are offset with respect to scalar (pressure, concentration) nodes. A fully implicit time-stepping scheme is used in conjunction with the SIMPLE algorithm [10].

Preliminary computations which were performed using a computational domain including the entire system showed that the solutions were symmetrical about the geometrical symmetry axis ($x = 10$ mm). Consequently, to reduce computational costs and storage, the computational domain used for all simulations covers only half the system, with the following boundary condition along the symmetry axis:

$$u=0,\quad \frac{\partial v}{\partial x}=\frac{\partial C}{\partial x}=0. \tag{9}$$

Table 1. Parameter values used in simulation of dissolution experiments

Dissolution experiment 1	
Density, ρ_0	6.434×10^3 kg m^{-3}
Diffusion coefficient, D	1.084×10^{-8} m^2 s^{-1}
Viscosity, μ	5.76×10^{-4} kg m^{-1} s^{-1}
Solutal expansion coefficient, β	-0.5907
Dissolution experiment 2	
Density, ρ_0	6.416×10^3 kg m^{-3}
Diffusion coefficient, D	1.101×10^{-8} m^2 s^{-1}
Viscosity, μ	5.75×10^{-4} kg m^{-1} s^{-1}
Solutal expansion coefficient, β	-2.11

The choice of a proper grid distribution poses several difficulties due to the unsteady nature of the problem and to the difference in molecular diffusion coefficients for momentum and mass transport. The Schmidt number for the solution is much larger than one, implying that the solute concentration boundary layers at the interfaces would be thinner than the momentum boundary layers [11]. Secondly, because of the time-dependent nature of the process, transient regions of high gradients will appear in various parts of the domain as time evolves, and in addition the thicknesses of the solute concentration and momentum boundary layers will change with time.

The grid distributions used in the present method were devised after a systematic grid sensitivity study in which grid refinement, grid expansion factors and rates of convergence were considered. These grid distributions consist of very fine cells clustered near the vertical walls where the velocity gradients are highest due to the formation of boundary layers. Grid refinement tests on a 71×29 grid and a higher density 101×41 grid yielded essentially identical results. The higher density grid was used for all results presented in this paper.

For each time step, the iteration cycle is terminated, and the time step is advanced when the normalized sum of the absolute differences between two successive space iterations is smaller than 5×10^{-5}, that is

$$\frac{\sum_{i=1}^{ni}\sum_{j=1}^{nj} |\phi_n(i,j) - \phi_{n-1}(i,j)|}{\sum_{i=1}^{ni}\sum_{j=1}^{nj} |\phi_n(i,j)|} \leqslant 5 \times 10^{-5} \tag{10}$$

where ϕ stands for u, v, p, and C, and n represents the number of iterations in space.

3. RESULTS AND DISCUSSION

3.1. *First dissolution experiment*

As solutal convection is due to the presence of concentration gradients, the variation with time of the averaged solute concentration profiles is first examined. Figure 2 shows that the concentration

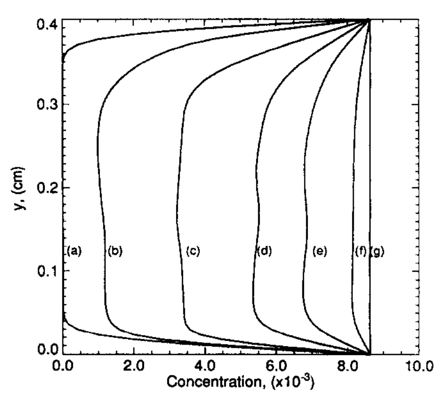

FIG. 2. Time variation of vertical distribution of solute concentration (profiles averaged in the x-direction). Time in seconds: (a) 1, (b) 10, (c) 29, (d) 61, (e) 99, (f) 213, (g) 3600.

gradients are initially identical at both substrates. These gradients decrease with time for both substrates. The rate of decrease at the lower substrate, however, is lower than that at the upper, resulting in higher concentration gradients and a thinner concentration boundary layer near the lower substrate. Dissolution causes a reduction in the density of the solution in the vicinity of the substrates, resulting in stable stratification in the upper region, and unstable stratification in the lower region. This in turn results in buoyancy induced upward motion of lighter silicon particles.

Figure 3 shows the computed flow and concentration fields in the left and right halves of the sandwich system respectively. Convection cells first appear near the lower corners, with upward velocities near the vertical walls. As time proceeds, the initial corner cells move towards the upper substrate, and weak secondary cells appear in the central region. A complex evolution of formation and amalgamation of secondary cells takes place during the first 200 s of the process. Throughout this phase convection dominates the lower region, whereas little fluid motion takes place near the upper substrate. After about 200 s, due to the reduction of the concentration gradients driving the motion, convection gradually dies out, becoming insignificant after about 800 s.

At the early stages of the process, the isoconcentrations are almost flat, typical of a mass diffusion phenomenon, except in the lower corners where isolated convective cells first appear. The straight isoconcentrations of the upper substrate are maintained for the whole duration of the process. In the lower region however, the strong interaction with the flowfield can be seen for $t \leqslant 200$ s. We notice first, that although the gradients near the upper substrate are gradually reduced, those along the lower substrate are maintained as a result of the upward motion of lighter silicon particles which depletes the solute in the lower region. Secondly, the concentration distributions are markedly non-uniform. As will be seen further, these distributions affect the substrate shape significantly.

A comparison of the experimental and predicted variations of the average dissolution depths is shown in Fig. 4. The overall agreement is quite satisfactory; in particular the simulations correctly predict the difference between the upper and lower substrates dissolution depths. The smaller dissolution depths achieved at the upper substrate indicate that melt saturation is achieved by silicon atoms originating mostly from the lower substrate. Solutal convection increases the upwards motion of silicon and enhances dissolution in the lower substrate.

Another important feature of the results is the much more rapid increase of the dissolution depths, on both substrates, during the initial period of the process. The In–Si solution is almost saturated within approximately 300 s (less than 10% of the total simulation time). The good agreement obtained with experiments

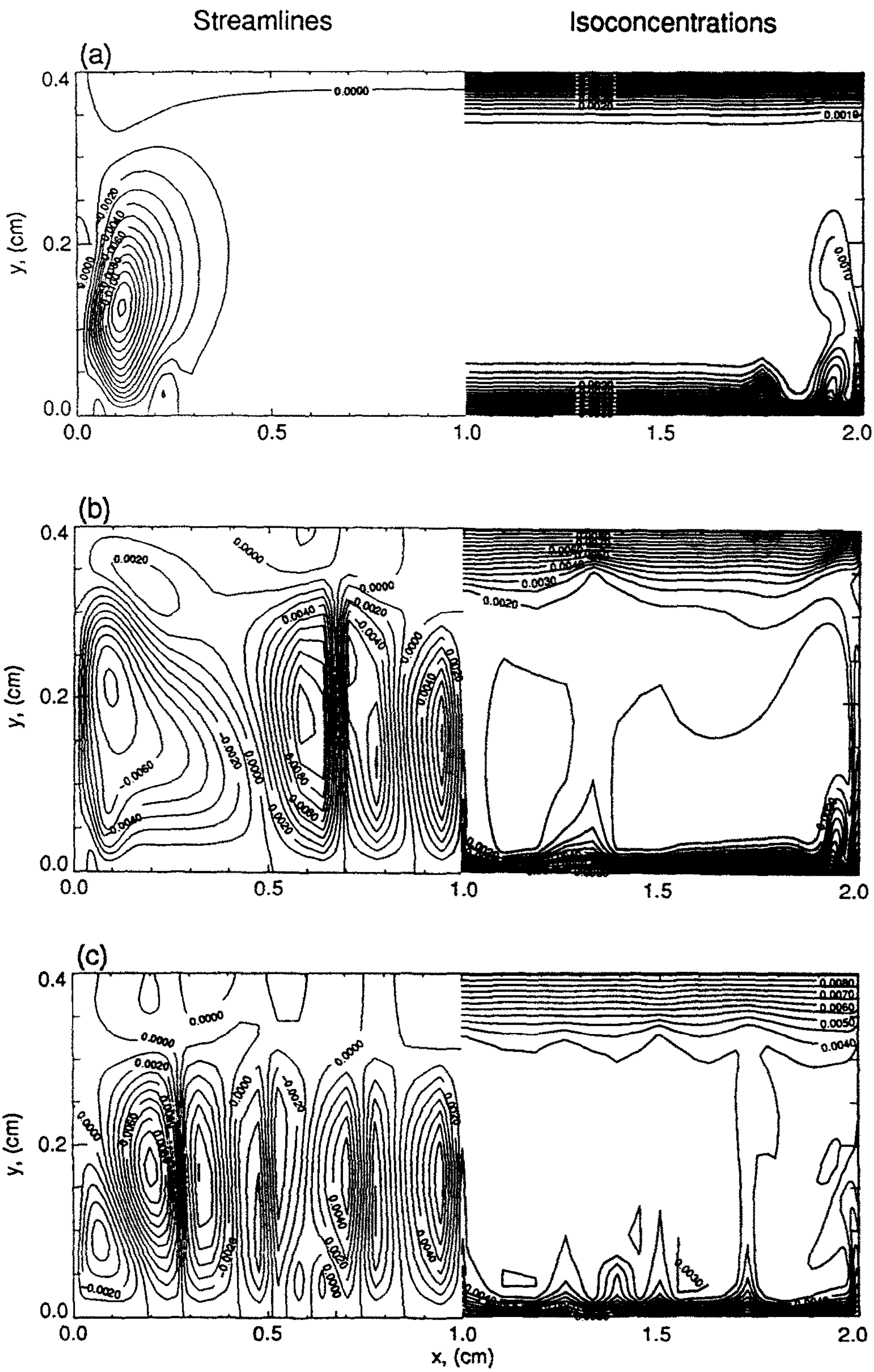

FIG. 3. Evolution of streamline patterns and isoconcentrations with time. Time in seconds: (a) 4.5, (b) 14, (c) 29, (d) 61, (e) 99, (f) 158, (g) 213, (h) 440, (i) 893.

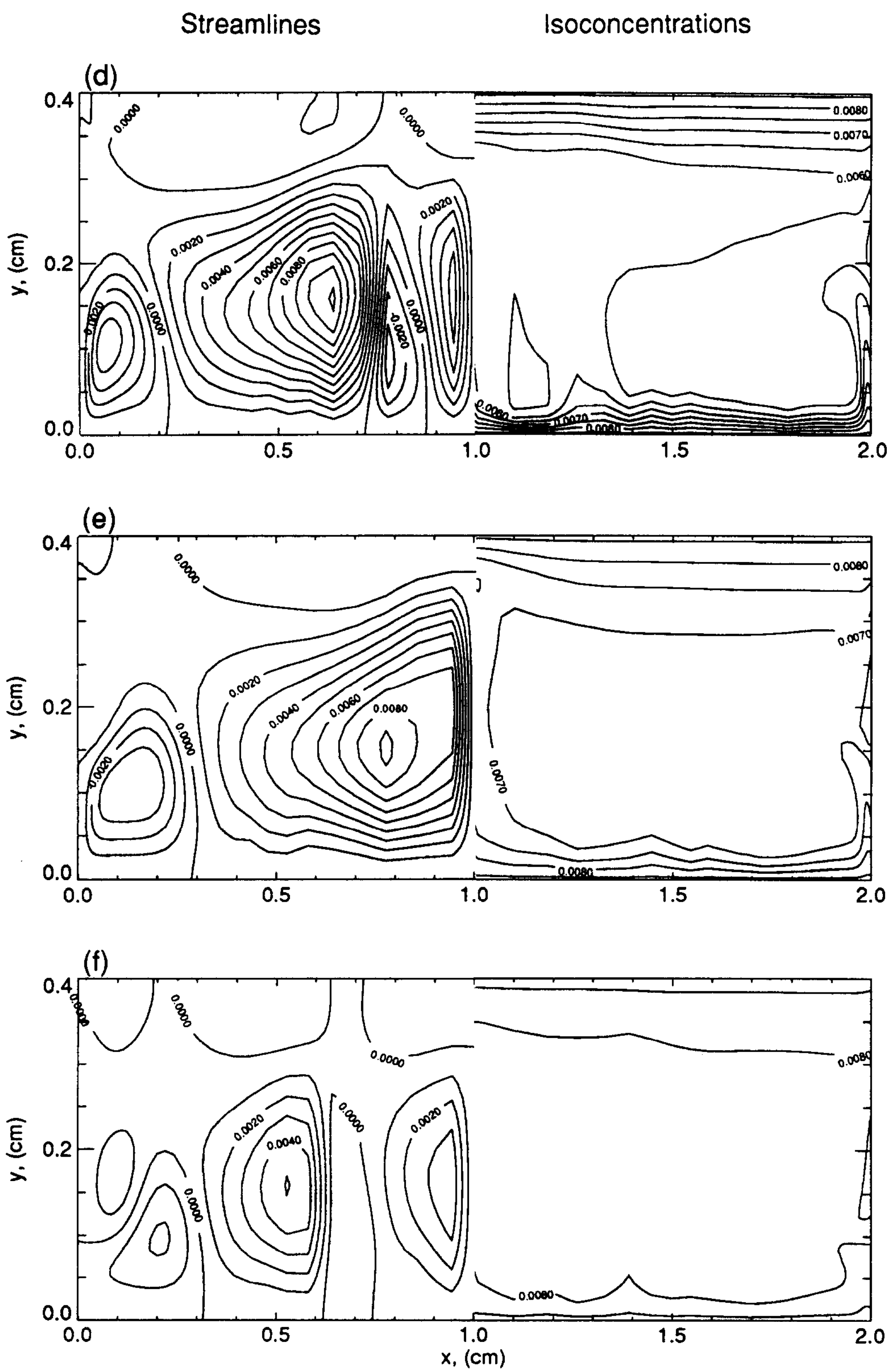

FIG. 3.—*Continued.*

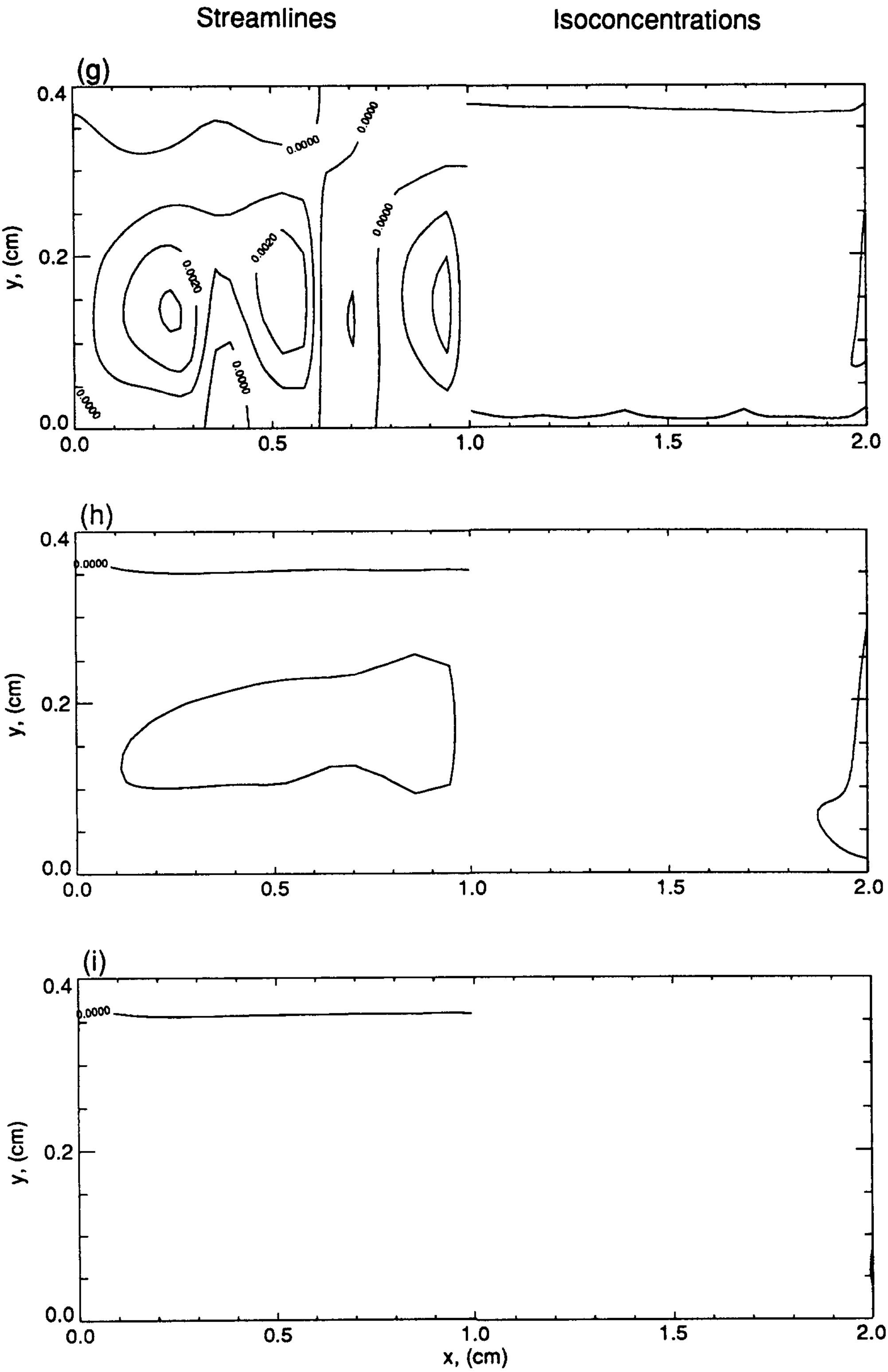

FIG. 3.—*Continued.*

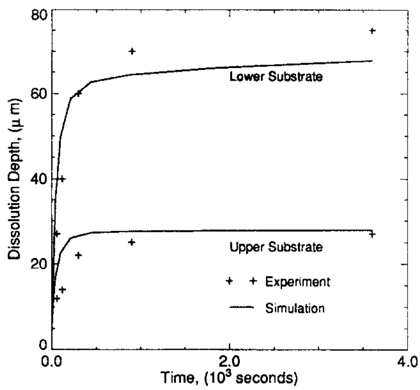

FIG. 4. Comparison of numerical and experimental dissolution depths.

confirms the importance of convective motion in this process. In particular, it should be pointed out that without convection the experimentally observed difference in the dissolution depths of the two substrates would not be predicted.

A more dramatic illustration of the effect of convection is the predicted shape of the substrate surfaces, shown in Fig. 5. While the upper substrate remains smooth and almost flat throughout the process, the lower substrate is wavy. This waviness arises from convective effects which dominate the process in the lower part of the domain in the initial phase and which are accompanied by the non-uniform concentration distributions noted in Fig. 3 along the lower substrate. The waviness increases during the first 300 s or so (corresponding to rapid dissolution in Fig. 4) of the process. The shape of the substrate remains essentially the same thereafter, with a uniform increase of the dissolution depth. The shape of the substrate near the walls is dictated by the development of concentration boundary layers on the side walls as illustrated in Fig. 6. Very sharp changes in concentration are present initially; the local concentration maxima and minima near the walls are gradually attenuated with time. No smoothing was used in Fig. 5, and spikes in the central portion correspond to grid points; the spikes are attenuated close to the walls of the dissolution cell where a much finer grid is used. The ragged shape also results in some uncertainty in the evaluation of the average dissolution depth.

The above results confirm that convection, which takes place in the presence of gravity, plays a major role in the dissolution process, and is responsible not only for higher dissolution depths, but also for wavy substrates. To further support these conclusions, simulations were carried out to investigate the effect of varying gravitational acceleration. The predicted dissolution depths for values from 1 to 10^{-2} g are shown in Fig. 7. As expected, the difference between the two dissolution depths is gradually reduced with decreasing g, until the two dissolution depths become

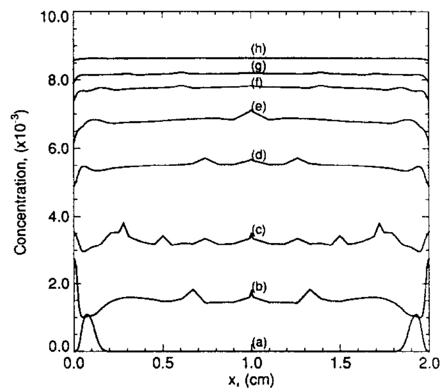

FIG. 6. Variation of solute concentration distribution at $y = 0.2$ cm. Time in seconds: (a) 4.5, (b) 14, (c) 29, (d) 61, (e) 99, (f) 158, (g) 213, (h) 3600.

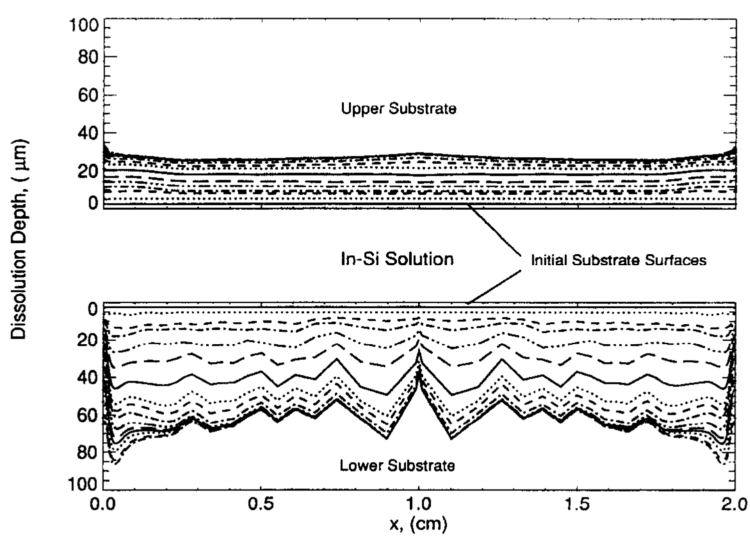

FIG. 5. Evolution of lower and upper substrate surfaces with time.

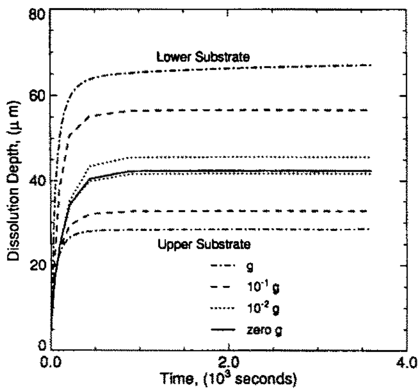

FIG. 7. Effect of gravity on dissolution depths.

identical in the absence of gravity ($g = 0$). No smoothing was used in plotting the reduced and zero gravity curves.

3.2. *Second dissolution experiment*

Quantitative experimental data are not available for this experiment, but the predicted difference between the upper and lower substrate depths is in qualitative agreement with the observations of ref. [6]. The simulations feature similar trends and characteristics to the first dissolution experiment. However, the predicted dissolution depths are about four times smaller, due to lower concentration gradients. The concentration gradients are a function of the difference between the initial and final solute concentrations. These vary from zero to approximately 8.63×10^{-3} for the first case, and from approximately 9.79×10^{-3} to 11.56×10^{-3} for the present case. The difference in concentration gradients is clearly seen by comparing Fig. 8 with Fig. 2.

In comparison to the previous case, the only significant difference in the shape of the substrate surfaces is a relatively smoother surface in the lower

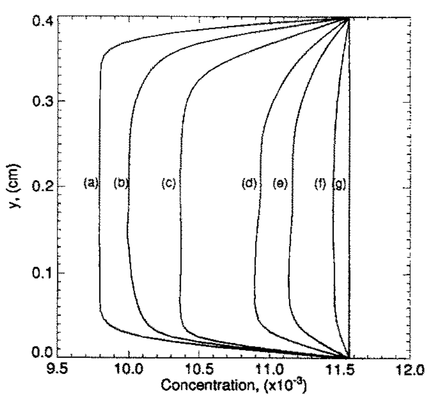

FIG. 8. Time variation of vertical distribution of solute concentration for dissolution experiment 2. Time in seconds: (a) 1, (b) 10, (c) 26, (d) 66, (e) 99, (f) 213, (g) 3600.

corners, as shown in Fig. 9. The smoother surface is due to the weaker concentration gradients along the vertical walls shown in Fig. 10. The weaker gradients are a consequence of the relatively weaker convection cells forming in the lower corners, and the thicker momentum boundary layers along the vertical walls which could be identified in the predicted flow patterns. These patterns exhibit the same gross features as in the first dissolution experiment and are therefore omitted for the sake of brevity.

As pointed out previously, there is some uncertainty in estimating the lower substrate average dissolution depth, due to the ragged surface. Numerical errors, due to the false diffusion inherent to upwind differencing schemes [12] contribute to uncertainties but would not affect the present results significantly, since high grid densities were employed. In addition, the uncertainty in evaluating some physical parameters is not critical to the present results either. For example, the diffusion and solutal expansion coefficient are changed by a factor of two when estimated by Long's method [13]. The use of these alternative values in the computations altered the predicted dissolution depths by a maximum of 10%.

4. CONCLUSIONS

The objectives of this study were to investigate the role of natural convection during the dissolution process. Numerical simulations which take into account both fluid flow and mass transport were presented for two dissolution experiments in a sandwich cell arrangement. The present solutal convection model is particularly useful in understanding some fundamental aspects of dissolution, and shows that convection, driven by concentration gradients in a gravitational field, plays a significant role in this process. The simulations show that natural convection is responsible for the experimentally observed differences in dissolution depths between top and bottom substrates, and clearly demonstrate that a model based only on diffusion would fail to reproduce this basic characteristic. An interesting consequence of the predominance of convective solution transport is the formation of a wavy substrate at the bottom, whereas the top substrate, where dissolution is controlled mostly by diffusion, remains smooth. This feature of the predictions has been recently confirmed by experimental observations [14].

In addition to clarifying the role of convection during the dissolution process, this study is a major stepping stone towards the next phase in which growth and dissolution will be combined cyclically to simulate the temperature modulation growth technique. These simulations will help evaluate the potential of this promising new growth technique.

Acknowledgements—The financial support of this research by the Canadian Space Agency (Users Development Program), the Japan Science and Technology Fund (External

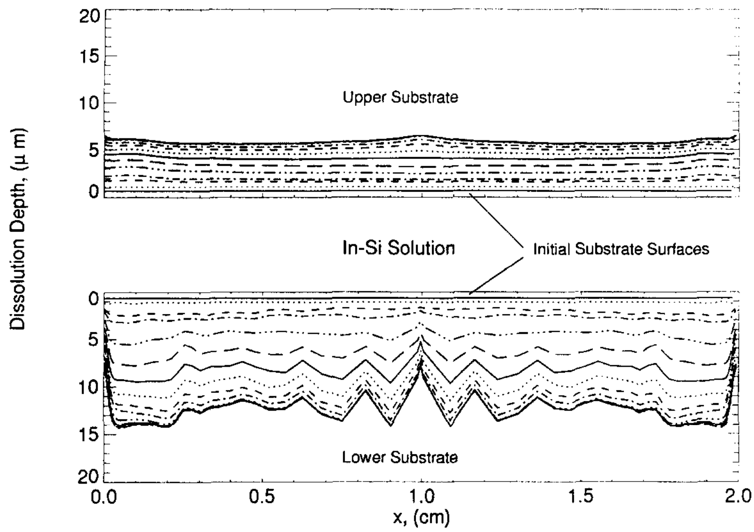

FIG. 9. Evolution of lower and upper substrate surfaces with time for dissolution experiment 2.

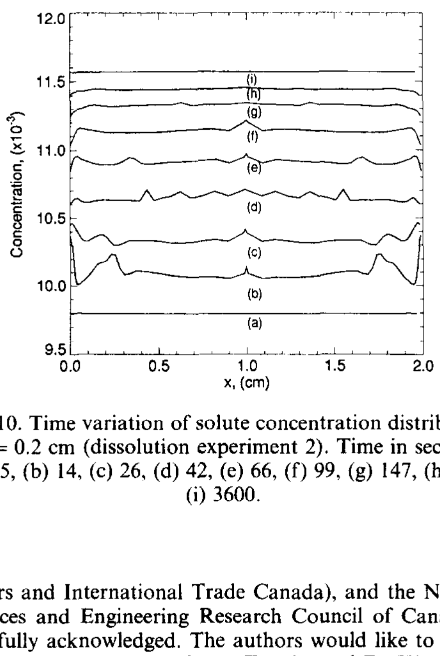

FIG. 10. Time variation of solute concentration distribution at $y = 0.2$ cm (dissolution experiment 2). Time in seconds: (a) 4.5, (b) 14, (c) 26, (d) 42, (e) 66, (f) 99, (g) 147, (h) 213, (i) 3600.

Affairs and International Trade Canada), and the Natural Sciences and Engineering Research Council of Canada is gratefully acknowledged. The authors would like to thank Professor Sukegawa, Professor Tanaka and Dr Kimura of the Research Institute of Electronics at Shizuoka University, Japan, for the exchange of information and stimulating discussions. Thanks are due to Mr Chris Gauld for his careful preparation of the Figures.

REFERENCES

1. S. Sakai, R. J. Matyi and H. Shichijo, Growth of GaAs-coated Si by liquid-phase epitaxy, *J. Appl. Phys.* **63**, 1075–1079 (1988).
2. H. Kanai, S. Motoyama, M. Kimura, A. Tanaka and T. Sukegawa, Gravity effect on liquid phase epitaxy of Si, presented at *Tenth Int. Conf. on Crystal Growth*, San Diego, Calif., 16–21 August (1992).
3. W. R. Wilcox, Computer simulation of growth of thick layers from solutions of finite solute concentration without convection, *J. Crystal Growth* **56**, 690–698 (1982).
4. J. D. Fehribach and F. Rosenberger, Analysis of models for two solution crystal growth problems, *J. Crystal Growth* **94**, 6–14 (1989).
5. S. A. Kassemi and S. Ostrach, Nature of buoyancy-driven flows in a reduced-gravity environment, *AIAA J.* **30**, 1815–1818 (1992).
6. T. Sukegawa, M. Kimura and A. Tanaka, Gravity effect on dissolution and growth of silicon in the In–Si system, *J. Crystal Growth* **92**, 46–52 (1988).
7. M. Kimura, A. Tanaka and T. Sukegawa, Gravity effect on solute transport in dissolution and growth of silicon, *J. Crystal Growth* **99**, 1295–1299 (1990).
8. C. D. Thurmond, Equilibrium thermochemistry of solid and liquid alloys of germanium and of silicon. I. The solubility of Ge and Si in elements of groups III, IV and V, *J. Phys. Chem.* **57**, 827–830 (1953).
9. W. R. Wilcox, Influence of convection on the growth of crystals from solution, *J. Crystal Growth* **65**, 133–142 (1983).
10. S. V. Patankar, *Numerical Heat Transfer and Fluid Flow*. Hemisphere, Washington, DC (1980).
11. F. Rosenberger, *Fundamentals of Crystal Growth I*. Springer, Berlin (1981).
12. G. D. Raithby, A critical evaluation of upstream differencing applied to problems involving fluid flow, *Comp. Meths Appl. Mech. Engng* **9**, 75–103 (1976).
13. S. I. Long, J. M. Ballantyne and L. F. Eastman, Steady-State LPE growth of GaAs, *J. Crystal Growth* **26**, 13–20 (1974).
14. M. Kimura, A. Tanaka and T. Sukegawa, Private communication (1992).
15. R. B. Bird, W. E. Stewart and E. N. Lightfoot, *Transport Phenomena*. Wiley, New York (1960).
16. C. J. Smithells, *Metal Reference Book* (5th Edn). Butterworths, London (1976).

APPENDIX: SYSTEM PARAMETERS

The equations used to compute the value of the parameters in Table 1 are given in this Appendix.

The liquidus relations for solutions formed by Si are represented by the following one-parameter equation [8]:

$$T[^{\circ}\mathrm{K}] = \frac{\Delta H + b(1-X)^2}{\Delta H/T_M - R\ln X} \tag{A1}$$

where, for an In–Si solution, the values of the parameter b, the heat of fusion ΔH, and the melting point T_M are given by:

$$b = 24.267 \text{ kJ g}^{-1} \text{ mol}^{-1}$$

$$\Delta H = 46.023 \text{ kJ g}^{-1} \text{ mol}^{-1}$$

$$T_M = 1703°\text{K}.$$

Using the relation between mass fraction and mole fraction [15], the liquidus relation can be written in terms of mass fraction C:

$$T[°\text{K}] = f(C).$$

This relation was inverted to a second order polynomial for the range of temperatures of interest by means of a least squares approximation:

$$C = 0.170716 - 0.386102 \times 10^{-3}\, T + 0.225563 \times 10^{-6}\, T^2 \tag{A2}$$

Due to lack of data, it is difficult to determine the density of In–Si solutions. Following Sukegawa *et al.* [6], the density of the In–Si solution is assumed here to decrease linearly with increasing concentration of Si, and to vary from the In value of the liquid phase to the Si value, yielding the following approximation:

$$\rho = \rho_{In} + C(\rho_{Si} - \rho_{In}). \tag{A3}$$

The densities of Si and In at the required temperatures are calculated following Smithells [16]

$$\rho_{In} = 7.028 \times 10^3 - 0.6798(T - T_M) \text{ kg m}^{-3} \tag{A4}$$

$$\rho_{Si} = 2.51 \times 10^3 - 0.32(T - T_M) \text{ kg m}^{-3} \tag{A5}$$

where the melting point temperature T_M is equal to 156.6°C for indium and 1410°C for silicon.

The solution under consideration is dilute; it is therefore assumed that the self-diffusion coefficient and viscosity of indium can be taken as the diffusion coefficient and viscosity of the In–Si solution. These are calculated using the following relations [16]

$$D = 2.89 \times 10^{-8} \exp\left(-\frac{1223}{T}\right) \text{m}^2 \text{ s}^{-1} \tag{A6}$$

$$\mu = 0.302 \times 10^{-3} \exp\left(\frac{1800}{T}\right) \text{kg m}^{-1} \text{ s}^{-1}. \tag{A7}$$

The solutal expansion coefficient is defined by

$$\beta = \frac{1}{\rho_0} \frac{d\rho}{dC}\bigg|_{C=C_0} \tag{A8}$$

β is then estimated based on the approximate relation (equation (A3)) for the solution density.